Surface & Coatings Technology 325 (2017) 370–376

Contents lists available at ScienceDirect

Surface & Coatings Technology

journal homepage: www.elsevier.com/locate/surfcoat

High deposition rate nanocrystalline and amorphous silicon thin film production via surface wave plasma source

Jason A. Peck [a,*], Piyum Zonooz [a], Davide Curreli [b], Gianluca A. Panici [a], Brian E. Jurczyk [c], David N. Ruzic [d]

[a] University of Illinois Urbana-Champaign, Department of Nuclear, Plasma, and Radiological Engineering, 105 Nuclear Radiation Laboratory, 201 S. Goodwin Avenue, Urbana, IL 61801, United States
[b] University of Illinois Urbana-Champaign, Department of Nuclear, Plasma, and Radiological Engineering, 116 Talbot Laboratory, 104 S. Wright Street, Urbana, IL 61801, United States
[c] Starfire Industries, LLC, 2109 S Oak St #100, Champaign, IL 61820, United States
[d] University of Illinois Urbana-Champaign, Department of Nuclear, Plasma, and Radiological Engineering, 101 Nuclear Radiation Laboratory, 201 S. Goodwin Avenue, Urbana, IL 61801, United States

ARTICLE INFO

Article history:
Received 12 January 2017
Revised 23 May 2017
Accepted in revised form 25 May 2017
Available online 25 May 2017

Keywords:
PECVD
Surface wave
Nanocrystalline silicon
Photovoltaics
Heterojunction

ABSTRACT

A 900 MHz surface wave antenna was used for plasma-enhanced chemical vapor deposition (PECVD) of silicon thin films in an $H_2 + SiH_4$ discharge, with an emphasis on photovoltaic applications. Gas mixtures of 0.7–10% SiH_4 at medium pressure (~100 mTorr) were tested with an optimal substrate temperature of 285 ± 15 °C, producing nanocrystalline hydrogenated silicon (nc-Si:H) at rates up to 3 nm/s, while amorphous films were grown in excess of 10 nm/s. A sharp transition from crystalline to amorphous growth was seen as SiH_4 flowrate increased, as is characteristic of silane PECVD. Increasing both substrate temperature and source power served to move this transition to higher flowrates, and by extension, higher deposition rates for the crystalline phase. Grain size also increased with substrate temperature, ranging from 10 ± 2 nm at 200 °C up to 15 ± 3 nm at 400 °C. Electron spin resonance showed that a-Si:H films grown via SWP were of acceptable defect density (~10^{16} cm^{-3}) and conductivity (~10^{-8} S/cm). Conversely, nc-Si:H films were poor quality (~10^{18} cm^{-3} defect density, 10^{-3}–10^{-2} S/cm conductivity) due to low hydrogenation and small grain size.

1. Introduction

Silicon thin films have been of interest for solar applications for decades, as they were the first commercially-viable photovoltaics (PV) produced [1]. Through the creation of a p-i-n junction, scattered photons can excite a current driven by the band structure of the device, allowing for the conversion of light into electricity. However, despite the low cost of production, the low efficiency of Si PV has driven industry to look to other materials [2]. One method to increase efficiency is to produce heterojunction cells—a layered device composed of materials with different bandgap energy E_g—to harness different sections of the solar spectrum. The materials must also be low defect, as impurities and dangling electron bonds serve as scattering centers for excited electrons to recombine and become lost, dropping efficiency.

Conveniently, two phases of hydrogenated silicon, amorphous (a-Si) and micro/nanocrystalline (μ/nc-Si), can satisfy these requirements, with E_g of 1.7 and 1.1 eV respectively [2]. While a-Si is very easy to produce rapidly via RF capacitively-coupled plasma (RF-CCP), industry standard for depositing low-defect μc-Si is rather low, with acceptable processes above 1 nm/s only recently being realized [3]. This is a detriment to production cost when the μc-Si layer must be on the order of 1 μm. This limitation calls for a reexamining of the deposition method.

The focus of this work is threefold – to characterize a surface wave plasma (SWP) source for the production of silicon thin films that are:

- high deposition rate,
- high quality/low defect, and
- flexible in process conditions between a-Si and nc-Si for the production of heterojunction devices.

It is believed that a surface wave plasma is ideal for this purpose. SWP sources employ ultra-high frequency (UHF) to excite a plasma. As the plasma reaches a sufficient density to screen the microwave, it reflects between the plasma and antenna surface to effectively become a "lossy" waveguide. The low oscillation height of electrons in the UHF range results in a maintained low electron temperature, keeping sheath potential and unintentional ion bombardment low.

SWP sources produce high plasma density (n_e ~$10^{11–12}$ cm^{-3}) and low electron temperature (T_e ~1–3 eV), as shown in Fig. 1, translating to fast deposition and minimal film damage. Microwave frequencies also allow for large-area deposition, as source coupling is generally

* Corresponding author.
E-mail address: peck3@illinois.edu (J.A. Peck).

http://dx.doi.org/10.1016/j.surfcoat.2017.05.074
0257-8972/

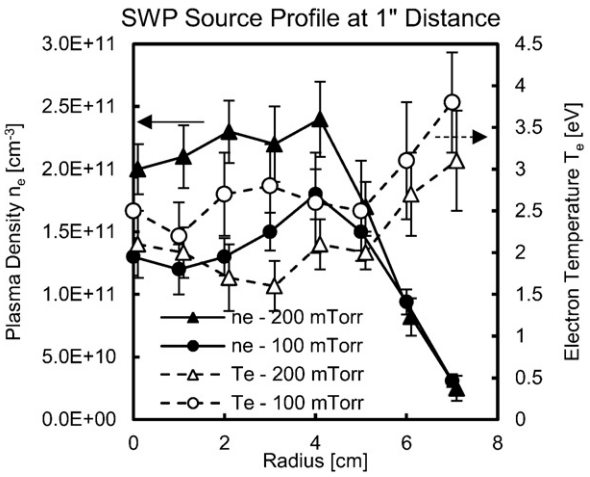

Fig. 1. Plasma density n_e and temperature T_e measured 25 mm away from the antenna surface. Fill pressures were 100 and 200 mTorr of H_2. Source power was 160 W at 900 MHz. Note that n_e roughly doubles as pressure is doubled, while T_e decreases with increasing pressure [4].

independent of chamber geometry or neighboring antennae [4]. Several groups have studied the eligibility of SWP for high rate PECVD [5–7,8,9], all showing advantages of high deposition rate (1–6 nm/s), PV-grade poly-crystalline Si due to the high n_e and low T_e properties of microwave SWP sources. Reactive PECVD through SWP has also been investigated, with SiN and SiO_2 growth possible even with remote plasma geometries [10,11]. Researchers such as Tadahiro Ohmi continue in developing microwave antennas for uniform, wide-area film growth, expanding into remote plasma etching sources as well [12].

Experimental exploration of the process space was accompanied with rigorous material diagnostics of the Si films, as well as numerical simulations of the $SiH_4 + H_2$ plasma discharge, correlating the deposition conditions with the films produced.

2. Experimental apparatus

The deposition chamber consisted of a 370 mm height × 370 mm diameter cylindrical cavity with a heated substrate on an adjustable bellows, which allowed for varying the discharge gap. The 180 mm surface wave antenna and 900 MHz microwave input were mounted to the top of the chamber, with dielectric backplate flush with the flange. The antenna and feedthrough were of proprietary design. Gas input was achieved via dual-ring manifold encircling the antenna, allowing for uniform gas input and radial diffusion to the center of the discharge. This apparatus is illustrated in Fig. 2.

Borosilicate glass coupons were used as a substrate for the H:Si films. To minimize variability at the beginning of the run, a high voltage DC supply assisted in instantaneous plasma breakdown so that minimal time was spent adjusting the matching network. Once deposition was complete, a chamber clean of 1:1 Ar + SF_6 plasma removed any deposited Si, 1:0.2 Ar + O_2 plasma removed any residual sulfates and organics, and finally Ar worked to clear out residual O_2.

3. Film analysis

3.1. Raman microscopy

Raman spectroscopy was effective in determining Si crystal fraction, alternatively referred to as Raman crystallinity. Using the Nanophoton RAMAN-11 Microscope, an incident 520 nm beam was scattered by the sample, exciting phonon modes in the material. Small changes in photon energy due to this inelastic phonon scattering, known as Stokes

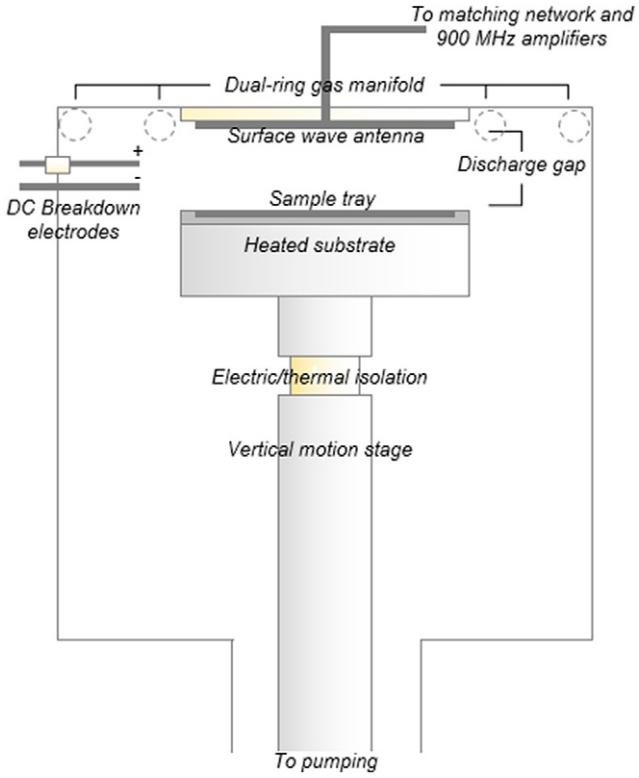

Fig. 2. Schematic of the UHF-SWP source and chamber.

shift, were measured, and the respective phonon spectra were determined.

The analysis of the Raman spectra followed a three-peak fitting centered around 480 ± 5 cm^{-1} (Gaussian), 520 ± 3 cm^{-1} (Lorentzian), and 500 ± 10 cm^{-1} (Gaussian), corresponding to amorphous, crystalline, and grain boundary contributions, respectively. The calculation of the crystal fraction follows from the ratio of integrated peak areas [13–15]:

$$fc = \frac{I_{520} + I_{500}}{I_{520} + I_{500} + c \cdot I_{480}} \quad (1)$$

where I is the area of each respective peak, and c is a weighting factor to compensate for improved absorption of the amorphous phase ($c \approx 0.7 - 0.9$ [15]; 0.8 was used in this work). This three peak fit was

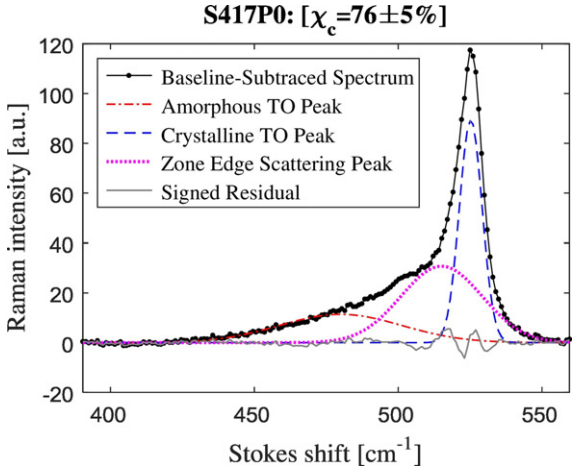

Fig. 3. (Color online) Peak-fitting of the 480, 500 ± 5, and 520 cm^{-1} contributions to the Raman spectra. The sample shown was calculated to be 76 ± 5% crystalline.

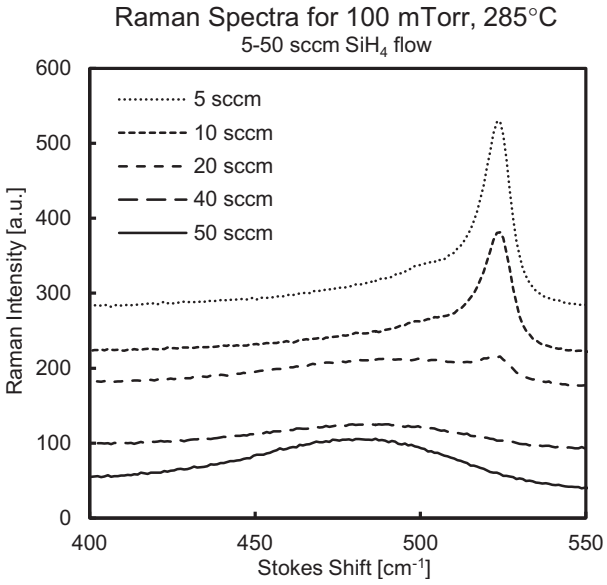

Fig. 4. Raman spectra for increasing SiH_4 flow. Silane concentration ranged from 0.7% (5 sccm) to 6.5% (50 sccm).

much more representative of the data and effective in reducing residual, in contrast to traditional 2-peak fitting of only 480 and 520 cm^{-1}. Analysis for a sample of relatively high crystallinity is shown in Fig. 3.

Fig. 4 demonstrates the emergence of the 500 ± 10 cm^{-1} nanocrystalline contribution, and eventually the 520 cm^{-1} TO c-Si mode at low silane concentration.

3.2. Temperature study

It was first necessary to optimize substrate temperature for process conditions. Interestingly, deposition rate was generally independent of substrate temperature. However, films deposited at low temperatures (<200 °C) were poorly-adhered and easily removed. SEM analysis of samples deposited at room temperature showed nanoparticles of 50–100 nm diameter; the presence of H:Si dust was attributed to low

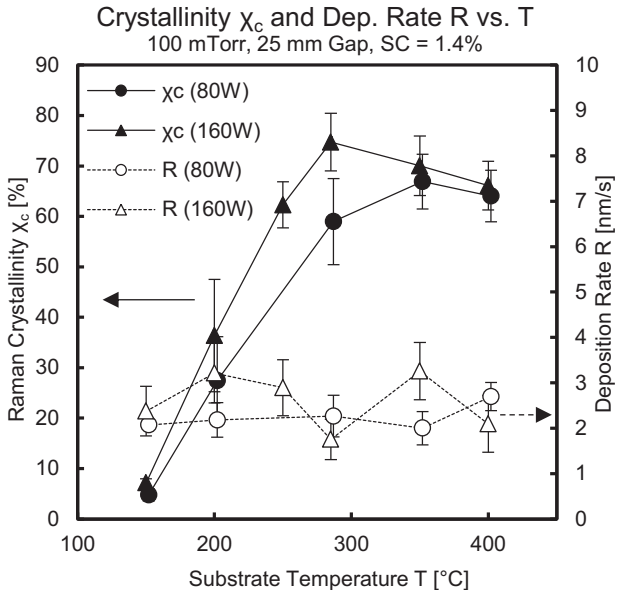

Fig. 5. Si film crystallinity χ_c (left axis), a.k.a. Raman crystal fraction, and deposition rate R (right axis) vs. temperature T. Fill pressure was 100 mTorr $SiH_4 + H_2$ with 1.4% silane concentration. 1.0 W/cm^2 microwave power and a 25 mm discharge gap were used.

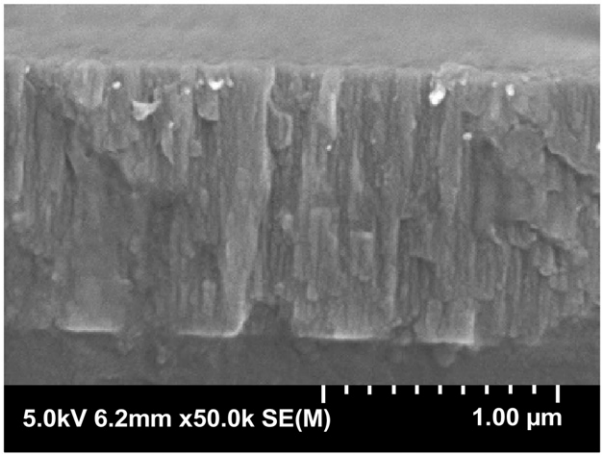

Fig. 6. SEM cross sectional image of nc-Si of 73 ± 6% crystallinity.

sticking probability of the substrate, promoting gas-phase particle formation instead.

It is observed in Fig. 5 that a maximum in crystal fraction occurs at 285 ± 10 °C for 160 W source power (or 1.0 W/cm^2). For 80 W (0.5 W/cm^2), this optimized temperature increases to 350 ± 10 °C. With sufficiently high substrate temperature, dense, vertically-structured films could be grown, as seen in Fig. 6, with an example of a-Si:H shown for comparison in Fig. 7.

Both the microwave power and the substrate temperature cooperate to increase crystal fraction. At lower temperature, deposited SiH_x radicals do not have sufficient thermal mobility to arrange into a crystalline structure. Netrvalová demonstrated this trend through measurement of XPS peak FWHM, signifying a growing crystallite size from 0 up to 150 °C [16]. In addition, Perrin [17] notes that the SiH_3 recombination process prevails over adsorption at lower substrate temperatures. This diminishes film quality as SiH_2 becomes the primary depositing species, growing very topically compared to SiH_3's diffusion into the film. On top of this, Kessels [18] has demonstrated the surface composition at low temperature (100 °C) is composed of primarily —SiH_2 and —SiH_3 bonds, while only —SiH sites appear at high substrate temperature, denoting efficient hydrogen removal and increased crystalline ordering at higher substrate temperature.

From varying SiH_4 concentration at 285 °C, the successful production of a-Si:H/nc-Si:H heterostructure is pictured in Fig. 8. While this structure consists of two layers of equal thickness, an optimized heterojunction photovoltaic would feature a much thinner a-Si:H layer with a thicker nc-Si:H layer, reflecting a-Si's significantly higher absorption coefficient.

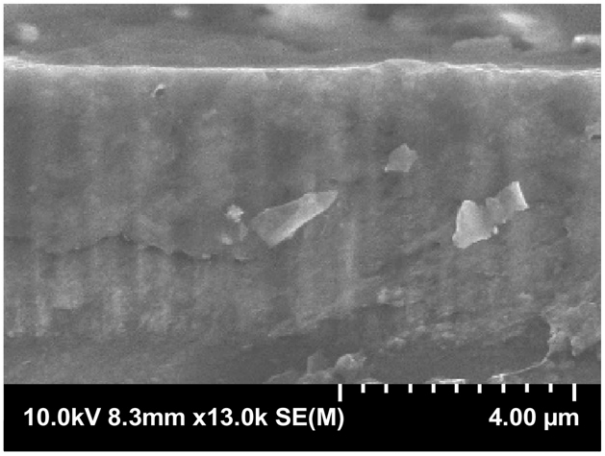

Fig. 7. SEM cross sectional image of a-Si with 21 ± 3% crystallinity.

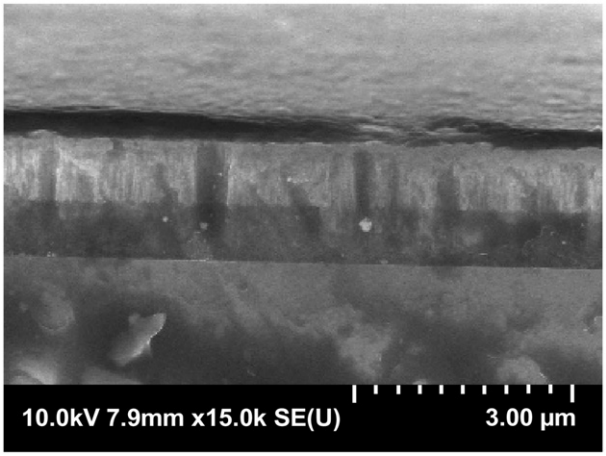

Fig. 8. Cross-SEM showing distinction between Si phases grown via SWP source – 1.0 μm nc-Si (75 ± 6% crystalline) atop 1.0 μm a-Si, grown on borosilicate substrate.

3.3. Pressure study

The influence of fill pressure was investigated with SiH_4 flow as the varied parameter. It is seen in Fig. 9 that the deposition rate does not vary with pressure below 100 mTorr. In fact, it is strongly linear with SiH_4 flow, denoting a relatively controllable process in regards to deposition rate. However, a higher pressure of 150 mTorr saw a slightly diminished deposition rate due to increased collisionality of SiH_x radicals.

The main distinction seen in Fig. 9 is that, at a low operating pressure of 25 mTorr, the transition from crystalline to amorphous films occurs at much lower SiH_4 flow. As fill pressure decreases, this results in both higher energy ions bombarding the surface and less H_2 radicals, since the H_2:SiH_4 ratio is lower. The former effect causes increased film damage, while the latter results in less surface Si—H bonds being broken, increasing film disorder through terminating Si early and preventing Si—Si bonding. This narrows the process window for nc-Si, constraining it to lower deposition rates and likely higher defect density. Thus, a higher operating pressure seems to both increase deposition rate and buffer out ion damage through collisions. This effect's influence on Si film growth by microwave plasma has similarly been reported by Ohkawara et al. [6].

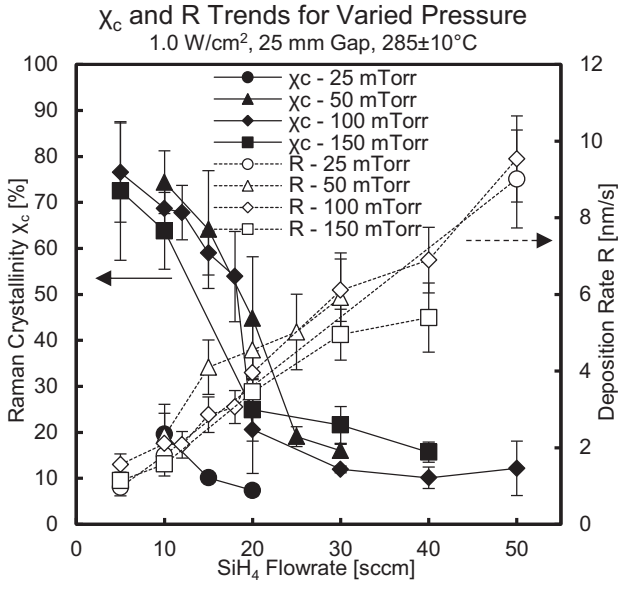

Fig. 9. Si crystallinity χ_c (Raman crystal fraction) and deposition rate R vs. silane flow for 25, 50, 100, and 150 mTorr fill pressure. Deposition conditions were 285 °C chuck temperature, 1.0 W/cm^2 microwave power, and a 25 mm discharge gap. Apart from diminished deposition rate at 150 mT and shifted crystallinity transition at 25 mTorr, trends are generally identical.

3.4. Power study

The addition of a second amplifier allowed for a wider range of microwave power to be investigated. The result, as seen in Fig. 10, demonstrates that the crystalline transition shifts from low SiH_4 flowrate at low power to higher flowrate at higher power. Increasing source power from 80 W (0.5 W/cm^2) to 160 W (1.0 W/cm^2) increased maximum nc-Si deposition rate from ~2 nm/s to ~3.5 nm/s.

On top of this, interpretation of Fig. 10 reveals another influencing factor in crystallinity. The linear trend of deposition rate vs. SiH_4 flowrate is unchanged with source power. This shows that the source's utilization of the process gas is very high, where doubling silane flow doubles deposition rate, even at half power. Thus, doubled power density produces more H radicals via dissociation instead. This surface treatment of monatomic hydrogen results in an abstraction reaction, removing the surface-passivating H-bonds that are an artifact of deposited SiH_x radicals. Increased hydrogen treatment *during deposition* will, ironically, decrease hydrogen content in the developing film, thus reducing disorder by allowing for surface-level Si—Si bonding, rather than Si—H termination, leading to crystallite growth. It may then be hypothesized that the crystal fraction is dependent on the ratio of H to SiH_x radicals incident on the surface (with SiH_2 being the dominant silane species). This has been confirmed recently by Hori [19] using time-dependent VUV absorption spectroscopy, and it has been roughly quantified for this SWP source via numerical modelling.

3.5. Grain size determination

To determine crystallite size, three techniques were employed—XRD, Raman analysis, and TEM. XRD spectra for varying substrate temperature are shown in Fig. 11. For X-ray diffraction, grain size was calculated via Scherrer equation [20]:

$$\tau = \frac{K\lambda}{\beta \cos\theta} \tag{2}$$

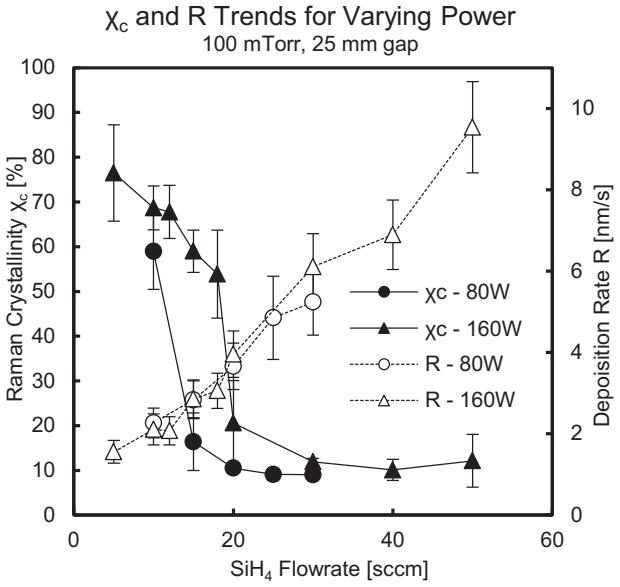

Fig. 10. Si crystallinity χ_c (Raman crystal fraction) and deposition rate R vs. silane flow for 80 W (0.5 W/cm^2) and 160 W (1.0 W/cm^2) source power. Note the rightward shift in crystalline transition for increasing μ-wave power.

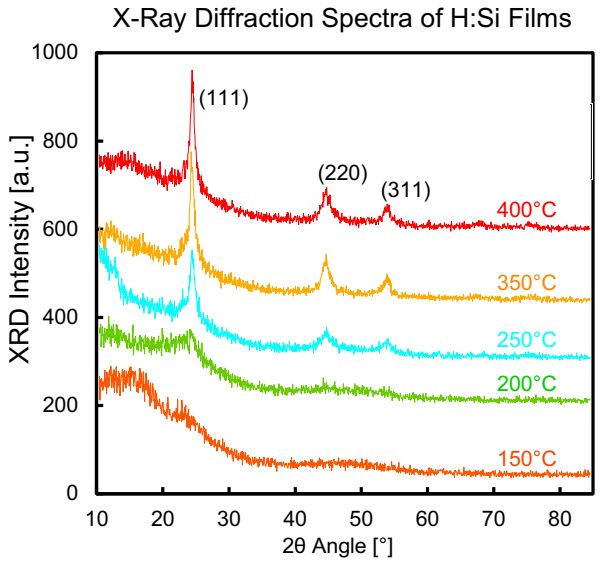

Fig. 11. (Color online) XRD spectra for H:Si at varied substrate temperature for 10 sccm SiH_4 flowrate.

where K is a shape factor ~0.89, λ is X-ray wavelength (Cu Kα, 0.154 nm), β is peak FWHM in radians, and θ is Bragg angle.

The average XRD grain size, as seen in Fig. 12, was determined to plateau around 12 ± 2 nm at 285 °C. The [111] contribution exhibited somewhat large grains in comparison, which may be overestimated based on the Raman analysis and TEM images that follow.

Raman calculation of grain size in Fig. 13, based on empirical fitting of the crystalline 520 cm^{-1} peak shift by Iqbal et al. [21] and ab initio calculations by Gao et al. [22], gives 6 ± 1 nm above 250 °C.

The TEM images in Fig. 14 are more in line with XRD averages of 10–15 nm grains. To perform TEM imaging, the top 10 nm of the Si films were polished away to exclude any oxide layer introduced by atmospheric exposure; they were then ion-milled to produce a "slice" of the top 20 nm, allowing for surface-normal imaging of the grain structure. In this way, the first ~10 nm of film growth, i.e. the "incubation layer", was also excluded, as grain size would be abnormally small in this region. Grain size calculation was performed through MatLAB image analysis to determine major and minor axes of these quasi-ellipsoidal grains.

While the TEM and XRD measurements are in good agreement, Raman calculations seem to underestimate grain size by a factor of 2.

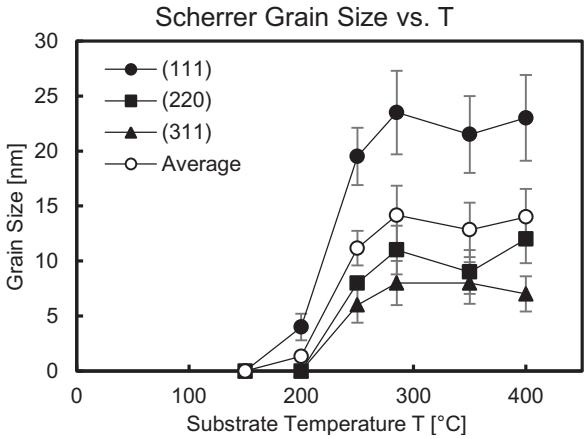

Fig. 12. Calculated grain size via Scherrer equation at 10 sccm SiH_4 for varying temperature. Average grain size for all orientations was done with weighted contributions from the area of each XRD peak.

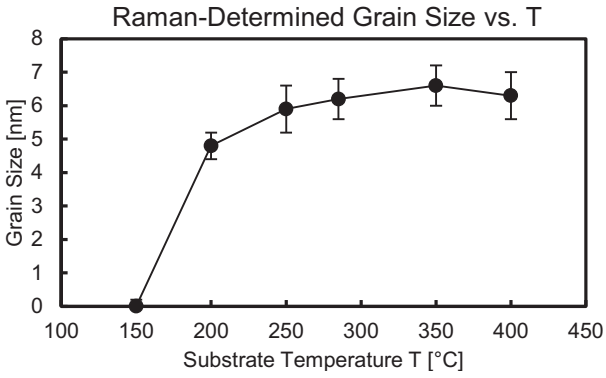

Fig. 13. Grain size, calculated from 520 cm^{-1} Raman peak broadening.

Regardless of characterization method, grain size is somewhat small for what would be desirable in photovoltaic applications. It is shown in the next section that this proves to be detrimental to nc-Si:H defect density and film conductivity.

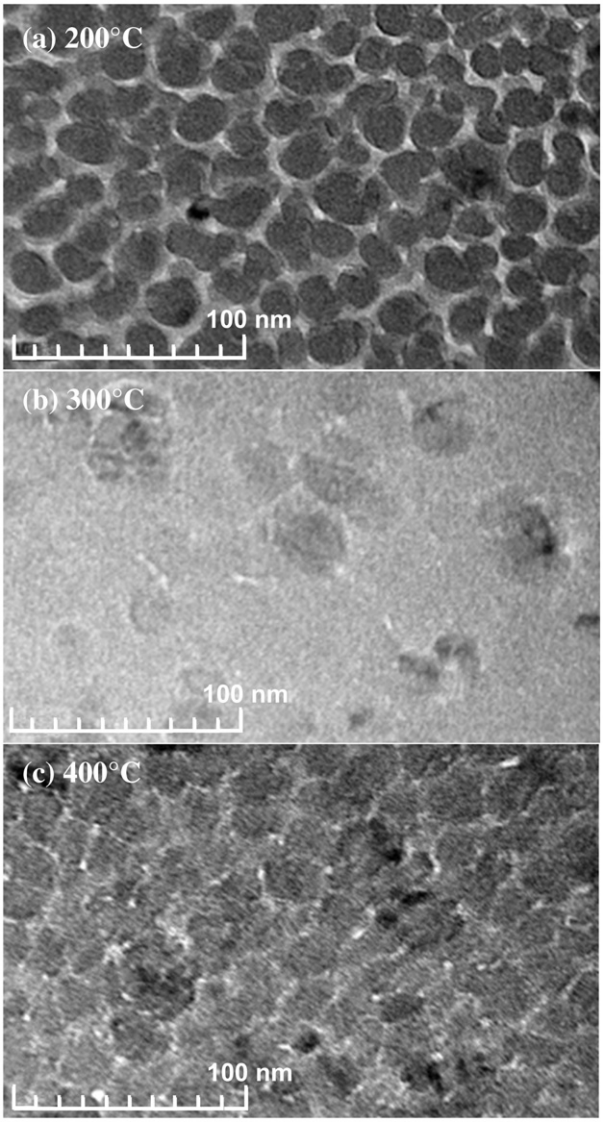

Fig. 14. TEM images of H:Si deposited with 10 sccm SiH_4 flow. Grain size estimates are (a) 10 ± 2 nm at 200 °C, (b) 13 ± 3 nm at 300 °C, and (c) 15 ± 3 nm at 400 °C. Note inter-grain amorphous zones reappearing at 400 °C. Grain sizes were estimated via MatLAB image analysis, approximating grains as ellipses and averaging major and minor axes.

3.6. Film quality

Electron spin resonance (ESR) was used to calculate the density of dangling bonds in the H:Si films. Moderately thick (~500 nm) films were deposited on quartz slivers and placed in a 3 mm quartz tube to be inserted in the active area of the ESR device. The resultant ESR absorption peak, centered around 3325 G, was compared against a 2,2-diphenyl-1-picrylhydrazyl (DPPH) standard, diluted 1:3100 in SiO_2 powder, to calculate spin density. The SWP-grown films were compared against RF-CCP-grown films for a relative comparison of the growth methods. The RF-CCP configuration duplicated SWP discharge gap dimensions and gas flow conditions by using the same chamber, employing a 15 cm diameter parallel plate with a 25 mm separation. 1.0 W/cm^2 power of 13.56 MHz excitation was applied to the live electrode while the coupon sat on the ground electrode. This guaranteed that the growing film wouldn't be subjected to the extreme DC self-bias.

It is seen in Fig. 15 that the surface wave source produces much lower defect density in comparison to RF-CCP at identical process conditions, most likely due to high hydrogen passivation of dangling bonds within the film. Staebler and Wronski [23] have shown that this H passivation is key to device performance. Only when crystallinity increases does defect density rapidly increase due to reduced hydrogenation of the film.

Despite the lower defect density for a-Si:H films, the source comparison Fig. 15 isn't particularly convincing of microwave SWP's advantages over RF, as typical RF-CCP processes employ much higher fill pressure to decrease ion damage due to increased collisionality. However, several groups [5–7] have demonstrated that increasing fill pressure similarly reduces defect density of SWP films, achieving as low as 10^{-16} cm^{-3}, even for microcrystalline samples. Thus, it is in our future interest to record defect densities of films deposited at increased operating pressure to further establish SWP's competitiveness against processes of record for RF-CCP.

In addition to defect density, dark and photoconductivity measurements were taken in order to understand electronic performance.

Compared to the ESR defect density's 2 order of magnitude increase, the dark conductivity in Fig. 16 changes much more rapidly, from a-Si:H ($1.6 \cdot 10^{-8}$ S/cm) to nc-Si:H ($9.5 \cdot 10^{-2}$ S/cm). The a-Si:H properties are comparable to what is achieved in literature [24,25]. The poor nc-Si:H quality, however, may be redeemed by high pressure re-hydrogenation post-deposition, as noted in Kuo's text [26].

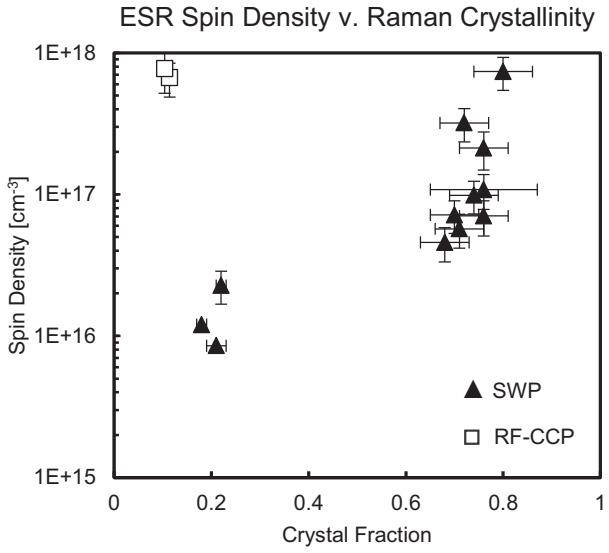

Fig. 15. ESR dangling bond density in H:Si films deposited via RF-CCP and SWP at 25 mm gap, 1.0 W/cm^2 power, 285 °C substrate temperature.

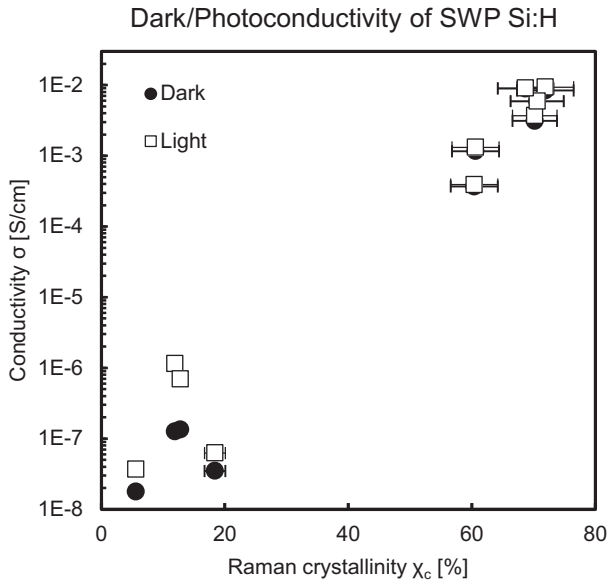

Fig. 16. Conductivity of H:Si films deposited via SWP at 25 mm gap, 1.0 W/cm^2 power, 285 °C substrate temperature. A Newport solar simulator was used for photoconductivity (white).

Coupling defect density data with film conductivity, it is apparent that SWP-grown a-Si:H has superior quality over nc-Si:H due to the rate at which it is grown, with hydrogen being incorporated into the film from deposited SiH_x. With higher SiH_4 dilutions required for producing nc-Si:H, silane radicals become increasingly dissociated by the plasma ($SiH_3 \rightarrow SiH_2$, SiH), while H radicals continue to abstract hydrogen from the film. As a result, grain boundaries are unpassivated, the defect density is significantly higher than a-Si:H, and conductivity skyrockets.

4. Conclusions

The optimization of a microwave surface wave plasma source was achieved, with a flexible process window allowing for high deposition rate (1–3 nm/s) nc-Si:H, albeit low-quality. However, we showed the ability to deposit a-Si:H at much higher rates (~10 nm/s) which exhibited promising material characteristics (low dangling bond density, low dark/photoconductivity), while nc-Si:H showed poor PV film quality—high defect density, small grains (10–15 nm), and high intrinsic conductivity. Higher source power was shown to reduce the optimal substrate temperature, relaxing the constraints on eligible substrate materials. As Si:H deposition rate scaled linearly with increasing SiH_4 flow, the aim of optimizing substrate temperature, total pressure, and SWP source power was to expand the crystalline transition into higher SiH_4 flow regimes to increase deposition rate.

With the assessment of grain size, conductivity, and defect density in hand, the next step is to test nc-Si:H growth processes at higher fill pressure, striving for grain boundary-passivated films that can be manufactured into an a-Si/nc-Si heterojunction cell. It must be cautioned that for any promising properties of these Si films, it will be necessary to verify material quality through p-i-n device performance.

Acknowledgments

The authors would like to thank Starfire Industries, LLC for their support. This project was also part of the NSF I/UCRC Center of Laser and Plasma for Advanced Manufacturing (CLPAM). For material diagnostics, we would like to thank the Frederic Seitz Materials Research Lab and the Electron Paramagnetic Research Lab at UIUC for facilities use and guidance.

This work is partially funded by the National Science Foundation under Grant No. IIP-1127557. Any opinions, findings, and conclusions or recommendations expressed in this material are those of the author(s) and do not necessarily reflect the views of the NSF.

References

[1] M.A. Green, Silicon photovoltaic modules: a brief history of the first 50 years, Prog. Photovolt. 13 (2005) 447–455.
[2] T.M. Razykov, C.S. Ferekides, D. Morel, E. Stefanakos, H.S. Ullal, H.M. Upadhyaya, Solar photovoltaic electricity: current status and future prospects, Sol. Energy 85 (2011) 1580–1608.
[3] H. Sai, K. Maejima, T. Matsui, T. Koida, M. Kondo, S. Nakao, Y. Takeuchi, H. Katayama, I. Yoshida, High-efficiency microcrystalline silicon solar cells on honeycomb textured substrates grown with high-rate VHF plasma-enhanced chemical vapor deposition, Jpn. J. Appl. Phys. 54 (2015), 08KB05.
[4] J.A. Peck, Modeling and experimental process optimization for a $SiH_4 + H_2$ surface wave plasma discharge for silicon photovoltaics, IDEALS dissertation and thesis databaseRetrieved from http://hdl.handle.net/2142/49498 2014.
[5] K. Yoshino, G. Ohkawara, H. Ueyama, H. Shirai, Fast deposition of microcrystalline silicon films with preferred (2 2 0) crystallographic texture using the high-density microwave plasma, Sol. Energy Mater. Sol. Cells 74 (2002) 505–511.
[6] G. Ohkawara, M. Nakajima, H. Ueyama, H. Shirai, Relationship between microstructure and photovoltaic performance in microcrystalline silicon film solar cells fabricated by a high-density microwave plasma, Thin Solid Films 427 (2003) 27–32.
[7] H. Jia, J.K. Saha, N. Ohse, H. Shirai, Effect of substrate bias on high-rate synthesis of microcrystalline silicon films using high-density microwave SiH_4/H_2 plasma, J. Non-Cryst. Solids 352 (2006) 3844–3848.
[8] H. Shirai, K. Yoshino, G. Ohkawara, H. Ueyama, Novel high-density microwave plasma utilizing an internal spoke antenna for fast deposition of microcrystalline silicon films, Jpn. J. Appl. Phys. 40 (2001) L701–L704.
[9] H. Tanaka, Z. Chuanjie, Y. Hayakawa, M. Hirayama, A. Teramoto, S. Sugawa, T. Ohmi, High-quality silicon oxide film formed by diffusion region plasma enhanced chemical vapor deposition and oxygen radical treatment using microwave-excited high-density plasma, Jpn. J. Appl. Phys. 42 (2003) 1911–1915.
[10] Y.-Y. Xu, T. Ogishima, D. Korzec, Y. Nakanishi, Y. Hatanaka, Deposition of SiN_x thin film using μ-SLAN surface wave plasma source, Jpn. J. Appl. Phys. 38 (1999) 4538–4541.
[11] K. Azuma, M. Goto, T. Okamoto, Y. Nakata, Low-temperature oxidation for gate dielectrics of poly-Si TFTs using high-density surface wave plasma, Electrochem. Soc. Proceedings 2003-2 2003, p. 614.
[12] T. Ohmi, M. Hirayama, A. Teramoto, New era of silicon technologies due to radical reaction based semiconductor manufacturing, J. Phys. D. Appl. Phys. 39 (2005) R1–R17.
[13] S. Gaïsler, O.I. Semenova, R.G. Sharafutdinov, B.A. Kolesov, Analysis of Raman spectra of amorphous-nanocrystalline silicon films, Phys. Solid State 46 (2004) 1528–1532.
[14] J.-D. Kwon, K.-S. Nam, Y. Jeong, D.-H. Kim, S.-G. Park, S.-Y. Choi, Control of crystallinity in nanocrystalline silicon prepared by high working pressure plasma-enhanced chemical vapor deposition, Adv. Mater. Sci. Eng. 2012 (2012) 213147.
[15] H.-S. Hwang, M.-G. Park, H. Ruh, H.-U. Yu, Investigations on microcrystalline silicon films for solar cell application, Bull. Kor. Chem. Soc. 31 (2010) 2909–2912.
[16] M. Netrvalová, M. Fischer, J. Mullerova, M. Zeman, P. Sutta, Structure and optical properties of the hydrogen diluted a-Si:H thin films prepared by PECVD with different deposition temperatures, The Eighth International Conference on Advanced Semiconductor Devices and Microsystems, Smolenice 2010, pp. 329–332.
[17] J. Perrin, Y. Takeda, N. Hirano, Y. Takeuchi, A. Matsuda, Sticking and recombination of the SiH_3 radical on hydrogenated amorphous silicon: the catalytic effect of diborante, Surf. Sci. 210 (1989) 114–128.
[18] W.M.M. Kessels, J.P.M. Hoefnagels, P.J. van den Oever, Y. Barrell, M.C.M. an de Sanden, Temperature dependence of the surface reactivity of SiH_3 radicals and the surface silicon hydride composition during amorphous silicon growth, Surf. Sci. Lett. 547 (2003) L865–L870.
[19] M. Hori, Y. Abe, A. Fukushima, Y. Lu, S. Kawashima, K. Miwa, K. Takeda, H. Kondo, K. Ishikawa, M. Sekine, Hydrogen radical-injection plasma fabricated microcrystalline silicon thin film for solar cells, Int. Plasma Chem. Soc. Ann. (Nagoya), 2013.
[20] A.L. Patterson, The Scherrer formula for X-ray particle size determination, Phys. Rev. 56 (1939) 978.
[21] Z. Iqbal, S. Veprek, A.P. Webb, P. Capezzuto, Raman scattering from small particle size polycrystalline silicon, Solid State Commun. 37 (1981) 993–996.
[22] Y. Gao, X. Zhao, P. Yin, F. Gao, Size-dependent Raman shifts for nanocrystals, Sci. Rep. 6 (2016) 20539.
[23] D.L. Staebler, C.R. Wronski, Refersible conductivity changes in discharge-produced amorphous Si, Appl. Phys. Lett. 31 (1977) 292–294.
[24] T. Zimmerman, High Rate Growth of Amorphous and Microcrystalline Silicon for Thin-film Silicon Solar Cells Using Dynamic Very-high-frequency Plasma-enhanced Chemical Vapor Deposition, Forschungzentrum Jülich GmbH, Jülich, GE, 2013 76.
[25] S.-I. Sato, H. Sai, T. Ohshima, M. Imaizumi, K. Shimazaki, M. Kondo, Photo- and dark conductivity variations of solar cell quality a-Si:H thin films irradiated with protons, IEEE Photovolatics Spec. 35 (2010) 2620–2624.
[26] Y. Kuo, Thin Film Transistors: Materials and Processes, first ed.vol. 2, Kluwer Academic Publishers, Norwell, MA, 2003 334.